"Preresidue" light charged particles from $^{28}Si+^{165}Ho$, $^{16}O+^{197}Au$, and $^{16}O+^{208}Pb$ fusion

B. J. Fineman, K.-T. Brinkmann,* A. L. Caraley, N. Gan, R. L. McGrath, and J. Velkovska
Physics Department, State University of New York at Stony Brook, Stony Brook, New York 11794
(Received 19 April 1994)

Proton and α-particle spectral shapes and multiplicities have been measured in coincidence with evaporation residues from 145 to 220 MeV $^{28}Si+^{165}Ho$ and 115 and 140 MeV $^{16}O+^{197}Au,^{208}Pb$ fusion reactions. Evaporation residues were separated using an electrostatic deflector and detected with large area surface barrier detectors. Light charged particles were detected at forward and backward angles with 14 single NaI detectors. In the context of the statistical model, the charged particle spectra provide information about the shapes and level densities of the emitting systems. Deformed emitters are inferred, and to a varying degree, an energy-dependent level density parameter is compatible with the data in each of the three cases. Implications for current fusion and fission dynamics studies are discussed.

PACS number(s): 24.60.Dr, 25.70.Gh

I. INTRODUCTION

A primary decay mode for an equilibrated compound nucleus (CN) involves light charged particle evaporation. While the statistical model (SM) has been used for many decades to analyze a variety of observables related to CN decay [1], the successful description of light particle emission remains essential for evaluating the validity of the model and the parameter choices within it. Studies of evaporated particle energy spectra yield direct information about the main SM ingredients, the nuclear level densities, and barrier penetration probabilities. Determination of these properties has application to current research into fusion and fission dynamics which often depends on the SM in some form for comparison to data.

Systematics collected during the 1950's and 1960's typically provide the starting point for SM calculations. From detailed balance, transmission coefficients (T_l's) for particle absorption are taken to describe particle emission. Most often, these come from optical model analyses of elastic scattering data. Studies of measured light particle spectra, focusing on peak positions and low energy shapes, have yielded varying conclusions concerning T_l's. In some cases, T_l's derived from OM systematics give acceptable results [2]; in others, reductions in charged particle emission barriers (typically by ~10%) are found necessary [3–6]. Alternative methods of calculating T_l's deemed more appropriate to particle evaporation have also been proposed [7,8].

For nuclear level densities, the most extensive information comes from slow neutron resonance data, at energies just above the neutron binding energy [1,9]. In SM calculations, level densities are routinely treated in an approximation to the Fermi gas model taking $\rho(U) \propto \exp(2\sqrt{aU})$ with level density parameter a. Calculations of the nuclear shape and size dependence of the level density parameter are available [10,11], but these provide for a "smooth" value, $\tilde{a}$, which does not account for fluctuations in a due to shell and pairing effects. To include these effects, several theoretical and phenomenological descriptions [12–14] show that above some critical energy (typically taken to be around 20 MeV) the effective excitation energy U should be calculated with respect to liquid drop ground state masses while at lower energies, a should be gradually varied from $\tilde{a}$ according to the shell and pairing energies of the particular nucleus. (One common form of such a description is presented in Sec. III A.) These treatments demonstrate a good understanding of the $\tilde{a} \approx A/8$ or $A/9$ $(\mathrm{MeV})^{-1}$ dependence [9,15] which describes the low energy systematics.

However, the compound systems produced in heavy ion collisions can deviate significantly in excitation energy and angular momentum from those involved in the neutron resonance studies. Here light particle energy spectral shapes provide the major experimental information on level densities, but the situation is not as well understood. Figure 1 shows level density parameters used in recent SM descriptions of neutron, proton, and α-particle spectra in the literature from systems with initial excitation energy $25 < E^*_{CN} < 200$ MeV [2,3,6,8,16–24]. Not only are there fewer such studies over the entire A range, but there are some significant deviations from the known $\tilde{a} \approx A/8$ or $A/9$ $(\mathrm{MeV})^{-1}$ forms valid near the neutron binding energy. This implies some energy dependence in $\tilde{a}$, even when it has not been included explicitly in the descriptions. A variation in $\tilde{a}$ with energy (or equivalently with temperature, $T \approx \sqrt{U/a}$) is not surprising and some energy-dependent forms have been used [8]. There are theoretical predictions for such effects [25,26], derived considering the variation with temperature of the nuclear size, surface diffuseness, and effective

*Present address: Technische Universität Dresden, Institut für Kern- und Teilchenphysik, Mommsenstr. 13, Dresden, Germany.

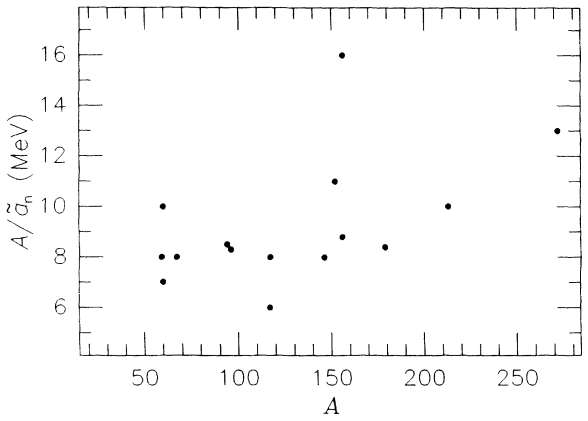

FIG. 1. Level density parameters taken from the literature extracted from neutron, proton, and/or α-particle spectral shapes from systems with initial excitation 25 MeV $\leq E^*_{CN} \leq$ 200 MeV.

mass. At higher temperatures $2 < T < 6$ MeV some experimental support for this behavior has been found [25,27,28]. (Other work [18] has failed to find conclusive evidence for the specific T dependence predicted in [26].) As the experimental situation is by no means clear below $E^*_{CN} = 200$ MeV and since data for heavy systems are particularly lacking, further experimental attention to such systems is desirable.

Furthermore, uncertainty in these issues influences conclusions about nonstatistical effects when SM calculations are used as a benchmark. In one application, Hinde *et al.* [29], in extracting dynamical fission delay times from prefission neutron multiplicities in the $A \sim 200$ region, note the sensitivity of their results to the value of the equilibrium level density parameter ($\tilde{a}_n$) used in the calculations. For example, changing $\tilde{a}_n$ from $A/8$ (MeV)$^{-1}$ to $A/10$ (MeV)$^{-1}$ significantly increases calculated prefission multiplicities, thereby reducing the extracted fission delay time by a factor of 2. The sensitivity to $\tilde{a}_n$ in calculations of prefission light charged particle multiplicities has also been discussed [30]. Recent attempts have been made to reduce these uncertainties through simultaneous measurements of prefission particle mean energies [31,32] but the theoretical values of $\tilde{a}_n$ of [11] were still relied on in these works. Additionally, as pointed out in [31,32], prefission data also require accounting for the complications of deformation-dependent variations in effective excitation energy, particle binding energies, and/or transmission coefficients along the entire path to scission.

In the present work, we have measured proton and α-particle energy spectra and multiplicities associated with evaporation residues (ER's) from three heavy systems, ^{193}Tl*, ^{213}Fr*, and ^{224}Th*, produced in heavy ion fusion reactions at moderate excitation energies between 60 and 130 MeV. These ER-gated data complement studies involving fission coincidences in the same mass and energy region [5,20,29–32] since the systems have relatively small angular momentum and do not cross the saddle point. Charged particles in coincidence with ER's are well suited for a detailed analysis in the context of the statistical model because the spectra are kinematically associated with a single source. This contrasts with the situation for singles or fission coincidence data which usually require deconvolution of components from several sources.

Evaporation residue cross sections for ^{28}Si+^{165}Ho were also measured and will be discussed in an appendix. These and previously measured ER cross sections for ^{16}O+^{197}Au, and ^{16}O+^{208}Pb [33] were used to constrain the SM calculations.

II. EXPERIMENT

Beams of 145 to 220 MeV ^{28}Si and 114 and 138 MeV ^{16}O were produced by the Stony Brook LINAC. The ^{165}Ho, ^{197}Au, and ^{208}Pb targets were 300 to 400 μg/cm^2 thick. Table I summarizes the reactions and excitation energies of the compound nuclei formed.

The setup for detecting evaporation residues was similar to that used previously for ^{16}O+^{197}Au,^{208}Pb residue cross section measurements [33]. ER's were separated from the beam by an electrostatic deflector and were identified in three 400 mm^2 silicon surface barrier detectors at 7°, 65 cm downstream from the target, using pulse height-TOF information. A 10 μg/cm^2 carbon charge reset foil was mounted 3 mm from the target to partially equilibrate ER charge state distributions.

Protons and α particles were detected in 5.1 cm × 3.8 cm NaI(Tl) detectors, 23 cm from the target and collimated to 3.8 cm. Six of these detectors were positioned around the beam axis at 165° for measuring the evaporative spectra in this work. Eight others were placed at various forward angles (48±15°) to study preequilibrium emission evident in the ER cross section data of Ref. [33]. The charged particles were separated from gamma rays and from each other by using both pulse shape-energy and TOF-energy discrimination [34]. ^{197}Au(p,p) elastic scattering and ^{6}Li(p,α) and ^{19}F(p,α) reactions at several energies were used for energy calibrations in advance of the actual data taking. A ^{228}Th α source was used as a monitor for gain shifts during the course of the data runs. As an added check for gain shifts, the mean proton and α-particle channel positions were computed for successive short run segments. Overall, the detectors were stable throughout the experiments to within ~±4% and no gain corrections were made.

The entire detector and deflector setup was modeled to determine efficiencies and explore the kinematic bias in the ER-light charged particle coincidence data. ER charge state distributions and small angle scattering in the target were determined via scans in deflector voltage as described in [33]. Coincidence efficiencies were

TABLE I. Reactions studied in the present work.

Projectile	Target	CN	E^*_{CN}
145,166,193,216 MeV ^{28}Si	^{165}Ho	^{193}Tl*	65,84,106,126 MeV
114,138 MeV ^{16}O	^{197}Au	^{213}Fr*	74,98 MeV
114,138 MeV ^{16}O	^{208}Pb	^{224}Th*	61,84 MeV

then calculated by a detailed trajectory tracing code [35]. This was necessary for finding particle multiplicities and possible distortions of the measured particle spectra. The calculations show that at back angles, spectral shapes are not affected significantly by the ER coincidence requirement. Reasonable variations of the parameters entering the efficiency calculations (describing, e.g., particle angular distributions and ER multiple scattering and charge state distributions) correspond to a ±25% and ±40% uncertainty in extracted proton and α-particle multiplicities, respectively.

An approximate description of the preequilibrium components of the spectra at forward and back angles was accomplished using incomplete fusion cross sections from the sum-rule model of [36] and a moving source description of particle emission [37]. The angular momentum-dependent cross sections calculated according to [36] were used as a starting point for further SM calculations to estimate preequilibrium particle yields in coincidence with associated ER's. These calculations indicate that contributions from incomplete fusion to the back angle spectra should be negligible but should dominate the forward angle spectra as observed.

The summed back angle center-of-mass energy spectra from protons and α particles gated by ER's from ^{28}Si+^{165}Ho, ^{16}O+^{197}Au, and ^{16}O+^{208}Pb fusion are shown in Figs. 2–5. Multiplicities are listed in Tables II–IV.

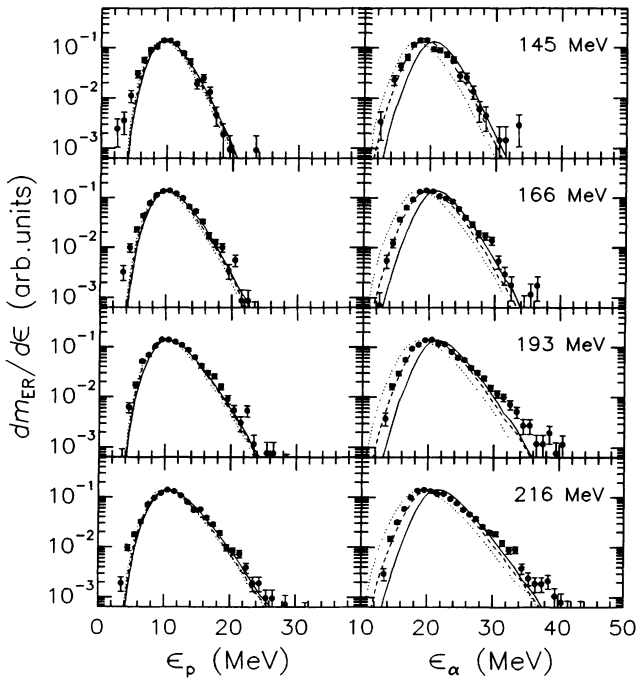

FIG. 2. Comparison of measured proton and α-particle spectra from ^{28}Si+^{165}Ho→^{193}Tl* with SM calculations assuming $\tilde{a}_n = A/9$ (MeV)$^{-1}$ and various emitter deformations: spherical emitter (solid curves), axis ratio 1.3 (dashed), and 1.5 (dotted).

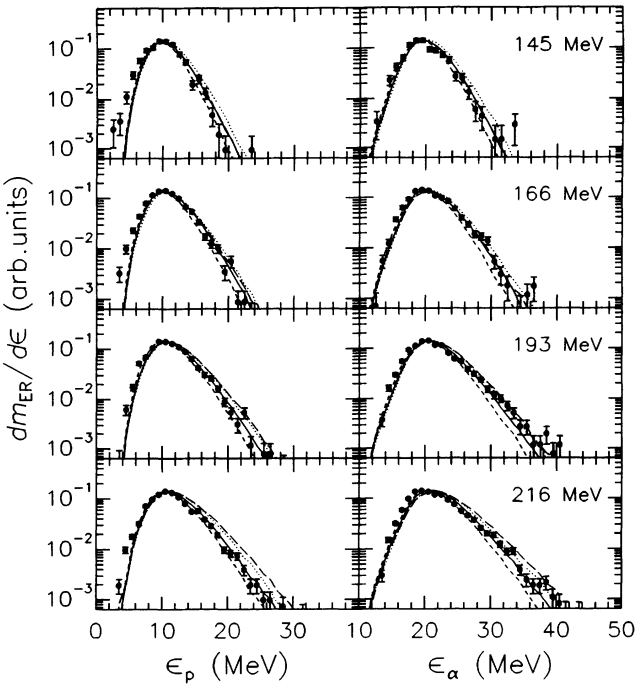

FIG. 3. Measured ^{28}Si+^{165}Ho→^{193}Tl* spectra as in Fig. 2, but with SM calculations assuming emitter axis ratio 1.3 and different level density forms $\tilde{a}_n = A/9$ (MeV)$^{-1}$ (short dashed), $\tilde{a}_n = A/11$ (MeV)$^{-1}$ (solid), $\tilde{a}_n = A/13$ (MeV)$^{-1}$ (dotted), and $\tilde{a}_n(U) = A/(8.2\text{ MeV} + 4.3\,U/A)$ (long dashed). Taking $\tilde{a}_n(U) = A/(8.2\text{ MeV} + 3.0\,U/A)$ gives results indistinguishable from the solid curves.

III. ANALYSIS

A. Statistical model calculations

A modified Monte Carlo version of the code CASCADE [38,39] was used to perform SM calculations. Fusion cross sections for ^{16}O+^{197}Au, and ^{16}O+^{208}Pb were taken as the sum of fission cross sections from

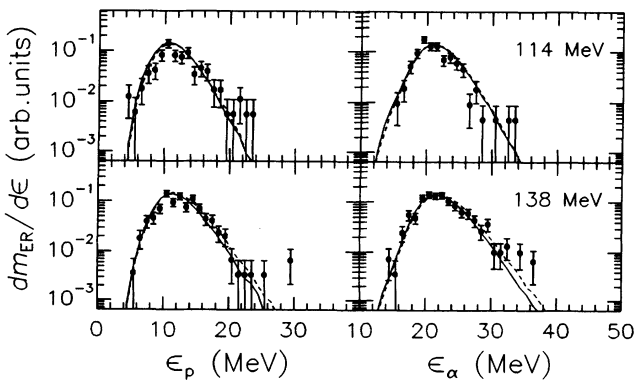

FIG. 4. Measured ^{16}O+^{197}Au→^{213}Fr* spectra with SM calculations assuming emitter axis ratio 1.3, and using $\tilde{a}_n = A/11$ (MeV)$^{-1}$ (solid) and $\tilde{a}_n(U) = A/(8.2$ MeV $+ 4.3\,U/A)$ (dashed) are shown.

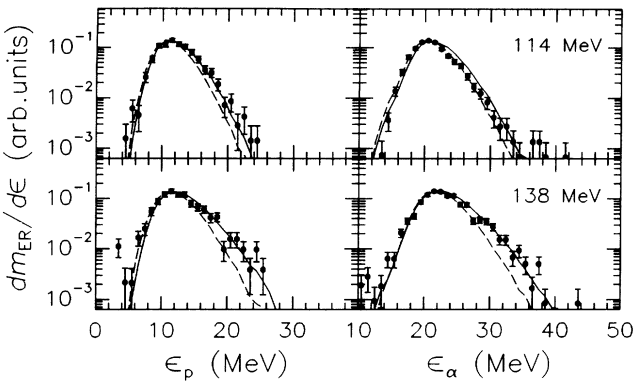

FIG. 5. Measured $^{16}O+^{208}Pb \rightarrow ^{224}Th^*$ spectra compared to SM calculations using $\tilde{a}_n = A/11$ $(MeV)^{-1}$ with emitter axis ratios 1.45 and 1.35 (dashed), and using $\tilde{a}_n(U) = A/(8.2\ MeV + 8.5\,U/A)$ with axis ratios 1.45 and 1.4 (solid). Calculations with $\tilde{a}_n = A/15$ $(MeV)^{-1}$ reproduce the solid curves.

[40] and [41], respectively, and residue cross sections from [33]. For $^{28}Si+^{165}Ho$, these were unavailable, so the fusion cross sections for the neighboring systems $^{28}Si+^{164,167,170}Er$ [42] were scaled and extrapolated. For reference, Table V lists these values for the reactions studied, and indicates the maximum angular momenta, J_{max}, which generate the fusion cross sections. (Triangular angular momentum distributions were used with 4 $\hbar$ diffuseness.) Essentially all the highest partial waves lead to fission so uncertainties in total fusion cross sections or partial wave distributions do not significantly affect the calculated ER cross sections or ER-related particle spectra.

Our initial "standard" calculations used the CASCADE optical model transmission coefficient routine for neutrons, protons, and α particles which relies on commonly used systematics [43–45]. We later modeled emitter deformation using the surface-area weighting approach of Huizenga *et al.* [46]. This involved averaging T_l's calculated for the varying radii along the surface according to their corresponding surface area fractions. Prolate shapes were assumed.

Level densities were calculated in a usual parametrization of the equidistant-level approximation of the Fermi gas model [47]. Whereas the original CASCADE routine treats the disappearance of shell effects in a linear interpolation scheme for the level density parameter, we chose

TABLE II. $^{28}Si+^{165}Ho$ measured and calculated proton and α-particle multiplicities. SM calculations use emitter axis ratio 1.3 and $\tilde{a}_n(U) = A/(8.2\ MeV + 3.0\,U/A)$. Uncertainties are discussed in the text.

E_{proj}	π_{ER} (exp.)	π_{ER} (SM)	α_{ER} (exp.)	α_{ER} (SM)
145 MeV	0.14±0.04	0.14	0.11±0.04	0.13
166 MeV	0.31±0.08	0.31	0.30±0.12	0.30
193 MeV	0.50±0.13	0.56	0.59±0.24	0.53
216 MeV	0.62±0.16	0.78	0.69±0.28	0.70

TABLE III. $^{16}O+^{197}Au$ measured and calculated proton and α-particle multiplicities. SM calculations use axis ratio 1.3 and $\tilde{a}_n(U) = A/(8.2\ MeV + 4.3\,U/A)$.

E_{proj}	π_{ER} (exp.)	π_{ER} (SM)	α_{ER} (exp.)	α_{ER} (SM)
114 MeV	0.14±0.04	0.12	0.17±0.07	0.18
138 MeV	0.41±0.10	0.30	0.46±0.18	0.49

to incorporate the more physical description presented by several authors [10,12,14,48]:

$$a_n = \tilde{a}_n \left[1 + \frac{\delta S}{U}\left(1 - \exp\frac{-U}{E_s}\right)\right],$$

with $U = E - E_{rot} + \delta P$. The shell and pairing energy corrections relate to the difference between empirical and liquid drop masses, $\delta S + \delta P = M - M_{LD}$, and the damping energy E_s was taken to be 18.5 MeV [10]. For a standard value, a constant $\tilde{a}_n = A/9$ $(MeV)^{-1}$ was used, close to that of [10,11] and in agreement with the neutron resonance systematics. To facilitate direct comparisons with related works in the literature, we began with the common procedure of keeping $\tilde{a}_n$ a constant, but varying it as a parameter.

For a more realistic description, we performed calculations using an energy-dependent $\tilde{a}_n(U)$, guided by the description of Shlomo and Natowitz [26] which follows a linear variation in (U/A) for the relevant energies involved here. From a curve shown in [26], we parametrized $\tilde{a}_n(U)$ as

$$\tilde{a}_n(U) = \frac{A}{8.2\ MeV + \kappa U/A}, \quad (1)$$

with $\kappa = 4.3$ fitting the results presented for $A = 210$ (similar to the masses involved in this work). This form also agrees with the systematic trend of the neutron resonance data, allowing us to test different energy dependences through modifications of the factor κ, without producing inconsistencies at low energies.

Rotational (yrast) energies were taken from the rotating liquid drop model (RLDM) [49]. These are very small for heavy systems, i.e., $E_{rot} \leq 5$ MeV for the partial waves leading to ER's, making the calculations insensitive to their precise magnitude.

Fission channel competition involves several other parameters whose effects are difficult to isolate. However, the ER-associated particles are not sensitive to the specific combination of fission parameters as long as the calculations yield the same ER cross sections. (Even large changes in the fission competition, which severely influence ER cross sections, correlate only loosely with

TABLE IV. $^{16}O+^{208}Pb$ measured and calculated proton and α-particle multiplicities. SM calculations use axis ratios 1.45,1.4 and $\tilde{a}_n(U) = A/(8.2\ MeV + 8.5\,U/A)$.

E_{proj}	π_{ER} (exp.)	π_{ER} (SM)	α_{ER} (exp.)	α_{ER} (SM)
114 MeV	0.13±0.03	0.12	0.22±0.09	0.32
138 MeV	0.27±0.07	0.29	0.56±0.22	0.52

TABLE V. Cross sections and related parameters used in the SM calculations (as described in text).

Reaction	σ_{CN} (mb)	J_{max}	σ_{ER} (mb)	k_f	$\tilde{a}_f/\tilde{a}_n$
145 MeV ^{28}Si+^{165}Ho	450	45	219	0.9	1.01
166 MeV ^{28}Si+^{165}Ho	920	70	214	0.9	1.01
193 MeV ^{28}Si+^{165}Ho	1000	70	156	0.9	1.01
216 MeV ^{28}Si+^{165}Ho	900	70	147	0.9	1.01
114 MeV ^{16}O+^{197}Au	1050	50	69	1.0	1.03
138 MeV ^{16}O+^{197}Au	1400	64	57	1.0	1.03
114 MeV ^{16}O+^{208}Pb	1150	52	8	0.9	1.04
138 MeV ^{16}O+^{208}Pb	1450	65	11	0.9	1.02

the preresidue particle spectral shapes.) The final values of the fission parameters used are listed in Table V. The parameters were chosen to best describe the magnitude and shape of the ER excitation function for each system, where possible parameter variation with energy was avoided for the sake of simplicity. They were varied within what we consider reasonable limits. The factor k_f scaling the fission barrier heights from the rotating finite range model (RFRM) predictions [50] was held within 10% of $k_f = 1$. The ratio $\tilde{a}_f/\tilde{a}_n$ of the saddle point to equilibrium shape level density parameters was kept within $1.0 < \tilde{a}_f/\tilde{a}_n < 1.1$, the range described in various experimental and theoretical determinations for heavy systems [10,11,51–53]. Fission time delays were not implemented in the standard calculations. (The discussion in the appendix provides some examples of how changes in fission parameters specifically influence ER cross sections for the ^{28}Si+^{165}Ho reaction.)

B. Comparisons with charged particle data

The standard SM calculations failed to describe adequately the measured proton and α-particle spectra. The calculated spectra are generally too soft. Furthermore, for α particles, the calculated spectra peak at higher energies than the data. It is found that including significant effective emitter deformation gives the correct peak energies and that modifications in the level density description lead to correct high energy slopes. We also show that without the constraint on the level density description from the neutron resonance systematics, the data here would not distinguish between the use of a constant $\tilde{a}_n$ and an energy-dependent $\tilde{a}_n(U)$. The forms which reproduce the data are described below and their plausibility and implications will be discussed in the next section.

Calculations for ^{193}Tl* with the standard value $\tilde{a}_n = A/9\ (\mathrm{MeV})^{-1}$ and a spherical emitter shape are compared to the data in Fig. 2. The effect of varying the emitter deformation (as exhibited in the T_l's) is illustrated using larger emitter axis ratios of 1.3 and 1.5 [while keeping $\tilde{a}_n = A/9\ (\mathrm{MeV})^{-1}$]. Deformation influences α-particle spectra more severely than it does proton spectra as observed previously [6,54]. A 1.3 axis ratio brings the calculation into good agreement with the low energy portion of the data. To describe the high energy slopes using a constant $\tilde{a}_n$, its value must be reduced. Calculations assuming axis ratio 1.3, but varying $\tilde{a}_n$ between $A/9\ (\mathrm{MeV})^{-1}$ and $A/13\ (\mathrm{MeV})^{-1}$, are shown in Fig. 3. The choice $\tilde{a}_n = A/11\ (\mathrm{MeV})^{-1}$, along with axis ratio 1.3 produces the best description of both proton and α-particle spectra at all four excitation energies. In the energy-dependent parametrization of (1), the theoretical energy dependence from [26], produces harder spectra than those measured for the higher beam energies (see Fig. 3). Using a reduced factor $\kappa = 3.0$, however, does result in satisfactory fits of the data which are essentially indistinguishable from the $\tilde{a}_n = A/11\ (\mathrm{MeV})^{-1}$ curves. The predicted charged particle multiplicities do not change dramatically with any of these variations, and agree with the data within the uncertainty of the efficiency determinations (see Table II).

The ^{213}Fr* particle spectra have poorer statistics which limit conclusions about the system. However, emitter deformation similar to that in ^{193}Tl* is clearly needed. This together with either a constant level $\tilde{a}_n = A/11\ (\mathrm{MeV})^{-1}$ or the energy-dependent $\tilde{a}_n(U)$ of (1) with $\kappa = 4.3$ (compatible with [26]) produces satisfactory results for spectral shapes and multiplicities (shown in Fig. 4 and Table III).

The ^{224}Th* spectra deviate more significantly from the predictions of the standard calculations. To describe the spectra, a larger effective emitter deformation appears necessary at 114 MeV than at 138 MeV. The $\tilde{a}_n = A/11\ (\mathrm{MeV})^{-1}$ or theoretical $\tilde{a}_n(U)$ level densities fail to produce hard enough spectra overall. Instead, either κ in (1) must be increased to 8.5, doubling the expected dependence of [26], or a very small constant $\tilde{a}_n = A/15\ (\mathrm{MeV})^{-1}$ must be used in order to reproduce the data. With either of these descriptions and emitter axis ratios 1.45 and 1.4, the calculations show good agreement with the spectral shapes and multiplicities. (See Fig. 5 and Table IV.)

Table VI summarizes the parameter descriptions which reproduce the charged particle data for the three systems.

C. Discussion

In light systems, reduced particle emission barriers are usually understood in terms of spin-dependent shape changes as predicted by the RLDM. In contrast, for the heavy systems studied here, RLDM predictions suggest almost spherical equilibrium shapes with axis ratios

TABLE VI. SM descriptions satisfactorily describing preresidue particle spectra in this work. (See text.)

CN	Effective deformation	Level densities
^{193}Tl*	1.3	$\tilde{a}_n(U) = A/(8.2\ \mathrm{MeV} + 3.0\,U/A)$ or $\tilde{a}_n = A/11\ (\mathrm{MeV})^{-1}$
^{213}Fr*	1.3	$\tilde{a}_n(U) = A/(8.2\ \mathrm{MeV} + 4.3\,U/A)$ or $\tilde{a}_n = A/11\ (\mathrm{MeV})^{-1}$
^{224}Th*	1.45, 1.4	$\tilde{a}_n(U) = A/(8.2\ \mathrm{MeV} + 8.5\,U/A)$ or $\tilde{a}_n = A/15\ (\mathrm{MeV})^{-1}$

≤ 1.1 for the angular momenta relevant to ER production. However, other effects may manifest themselves in heavier systems. Specifically, there may be significant nuclear shape fluctuations and/or dynamics not included in the SM description. The possibility of dynamical effects being involved in charged particle decay in this mass region has been discussed previously by several authors [55,56]. The picture of the equilibrated nucleus decaying from an equilibrium shape may be inadequate if particle emission occurs either during the composite nucleus formation stage or while the nucleus evolves toward the saddle configuration.

Fusion time scales were estimated for the reactions studied here to be $\sim 3\times10^{-21}$ s using Feldmeier's macroscopic model [57,58] incorporating one-body dissipation. While these times are an order of magnitude shorter than those expected for the more mass-symmetric system examined in [55], they are still comparable to the SM mean lifetimes calculated in CASCADE. (SM lifetimes range from about 1 to 10×10^{-21} s at the initial compound nucleus excitation energies.) Thermalization times should be negligible, shorter than the dynamical times by an order of magnitude [57]. Hence, statistical emission prior to full relaxation of the compound nucleus shape cannot be ruled out.

However, the large fissility of these systems and the magnitude of current estimates of fission delay times suggest that particle emission along the path to the saddle point may be most important. The $\sim 10\times10^{-21}$ s presaddle time delay determined by Lestone *et al.* [32] would allow charged particle evaporation from deformed shapes in a system "trying" to fission. The resulting reduction in fissility and excitation energy can significantly stabilize such a system, enhancing its probability for winding up in an ER channel. The fact that the larger effective deformations are evident in ^{224}Th*, the most fissile system studied here, supports this interpretation. This system was also produced with the most asymmetric reaction, again arguing against the dominance of entrance channel effects.[1]

It should be noted, however, that even in a static statistical picture, the deformations seen in the particle spectra may simply reflect a Boltzmann averaging over all possible configurations of the system. As pointed out by Gaardhøje [59], even at temperatures as low as $T \geq 1$ MeV, the sampling of a broad range of shapes in the rather flat potential energy surfaces of heavy systems can be considerable. The available energy is relatively unchanged even at the saddle point deformations for these systems, as indicated by the small fission barriers (zero angular momentum RFRM values are $B_f = 12$, 8, and 6 MeV, for ^{193}Tl*, ^{213}Fr*, and ^{224}Th*, respectively). Quantitative calculations of shape fluctuation effects for particle decay in these systems are not available at present; a more elaborate statistical code would be required than is currently implemented.

It is clear, therefore, that particle evaporation from deformed emitters is not surprising in this mass region. While the standard SM cannot distinguish between the various mechanisms which can produce this effect, it can successfully describe the data through the adoption of effective emitter deformations.

The nuclear level density descriptions used in this work are shown in Fig. 6 (calculated for ^{224}Th* here for illustration). In the SM, the variation of level density with daughter excitation energy, E_d^*, essentially determines the high energy shape of a particle spectrum. This follows from the direct relation between the particle energies ϵ and the parent and daughter excitation energies:

$$\epsilon = E_p^* - E_d^* - S,$$

with S specifying the particle separation energy. The spectral shape does not depend on whether a constant $\tilde{a}_n$ or an energy-dependent $\tilde{a}_n(U)$ is used if the resulting shapes of $\rho(E_d^*)$ are the same for the relevant range of energy. In the present reactions, since the high energy parts of the spectra are dominated by emissions from "first stage" decays, the energy range probed falls below the initial CN excitation energy, $E_{\rm CN}^*$, at roughly $(E_{\rm CN}^* - 30\ {\rm MeV}) \lesssim E^* \lesssim (E_{\rm CN}^* - 15\ {\rm MeV})$. For example, in Fig. 6, the $\tilde{a}_n(U) = A/(8.2\ {\rm MeV} + 8.5\,U/A)$ and $\tilde{a}_n = A/15\ ({\rm MeV})^{-1}$ descriptions show similar shapes in $\rho(E^*)$ between 30 and 70 MeV. Consequently, these produce similar particle spectral shapes for ^{224}Th* at the initial excitation energies produced. The acceptable descriptions determined for ^{193}Tl* and for ^{213}Fr* compare in the same manner.

To decide on the appropriate form, one must appeal to evidence from a broader energy range. The extensive neutron resonance systematics at low energy clearly favor $\tilde{a}_n \approx A/8$ or $A/9\ ({\rm MeV})^{-1}$ and so constrain the level densities in that region. The spectral shapes at higher energies then determine not only the $\rho(E^*)$ shape in a limited energy region, but also establish its magnitude and energy dependence over a wide range of excitation. The data presented in this work, therefore, support the energy-dependent $\tilde{a}_n(U)$ forms listed in Table VI.

The differences between the descriptions needed for the three systems are not understood. The $\tilde{a}_n(U)$ energy variation shown in [26] does depend somewhat on mass. In our parametrization (1), one expects κ would change by $\sim$15% over the limited mass range studied here. However, the data show a much larger variation for the three systems; κ varies by a factor of ~ 3. To further investigate these issues, more studies in this mass region and over a wider energy range are indicated.

One possible direction for future study involves the determination of the decay lifetimes for such systems us-

[1]Prefission proton and α-particle spectra from a system studied in the present work, ^{213}Fr*, were presented by Ikezoe *et al.* [20] and are suggestive of an even larger emitter deformation than determined for our preresidue data. In our calculations, an axis ratio of $\sim$1.7 is needed to describe the "compound nucleus" components of their prefission spectra. This is still well within the saddle point deformation (with axis ratio $\sim$2.3), but appears to support the idea that charged particle emission continues to occur while the compound nucleus evolves toward a saddle shape.

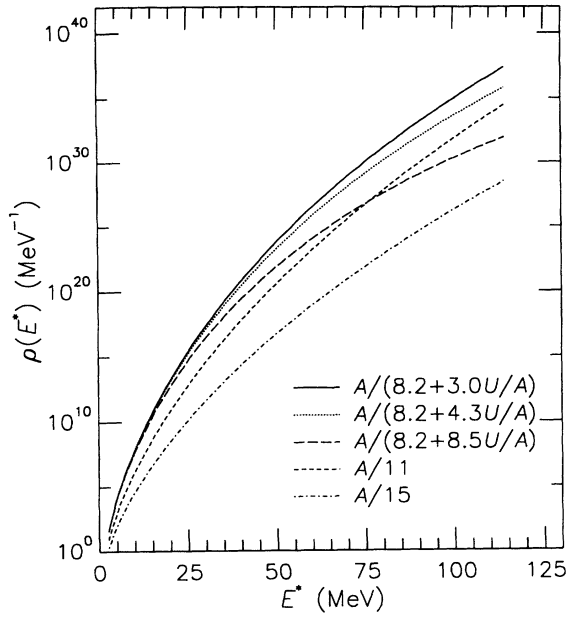

FIG. 6. Level densities for ^{224}Th* (at 20 $\hbar$) with the various level density forms described in the text: $\tilde{a}_n = A/11$ (MeV)$^{-1}$ (short dashed), $\tilde{a}_n(U) = A/(8.2\text{ MeV} + 3.0\,U/A)$ (solid), $\tilde{a}_n(U) = A/(8.2\text{ MeV} + 4.3\,U/A)$ (dotted), $\tilde{a}_n(U) = A/(8.2\text{ MeV} + 8.5\,U/A)$ (long dashed), and $\tilde{a}_n = A/15$ (MeV)$^{-1}$ (dot-dashed).

ing particle-particle small-momentum correlations [60]. In the SM, lifetimes derive directly from the total decay widths, potentially offering an additional tool for examining level densities. The level density forms with small constant $\tilde{a}_n$'s result in shorter mean lifetimes than those with standard values; the variable $\tilde{a}_n(U)$ forms produce lifetimes which are shorter still. As an example, for the ^{193}Tl* system at $E^*_{\rm CN} = 126$ MeV, the level densities which equally well describe the particle spectra, with $\tilde{a}_n(U) = A/(8.2\text{ MeV} + 3.0\,U/A)$ and $\tilde{a}_n = A/11$ (MeV)$^{-1}$, give significantly different SM lifetimes; at $J = 0$, these are 0.7×10^{-21} s and 1.4×10^{-21} s, respectively. Determination of the lifetimes may therefore provide new insight into nuclear level densities.

The present SM results have significant implications on current estimates of fission delay times. The effect of both the level densities and emitter deformations determined would be to enhance particle emission over fission competition compared to those in standard SM calculations. This would lead to shorter deduced fission delays needed to describe prescission light particle or γ-ray emission data. We should point out, however, that the extent of the variation in SM parameters seen even for the ER-associated data suggests that increasingly quantitative demands on the SM for these reactions may not be appropriate. The dynamical effects discussed above dictate the importance of calculations merging dynamics with statistical decay. Such treatments are beginning to appear in the literature [61,62].

IV. SUMMARY

We have measured evaporation residue-gated proton and α-particle energy spectra and multiplicities from ^{193}Tl*, ^{213}Fr*, and ^{224}Th* composite nuclei produced at moderate excitation energies. Results from all three systems suggest emitter deformation and so demonstrate the need to consider dynamical effects and/or nuclear shape fluctuations in a statistical model description of evaporative particle decay.

The measured spectra also exhibit harder shapes than those predicted by standard SM calculations. A satisfactory description of the data is obtained using either small constant level density parameters, or level density parameters with various energy dependences. Constrained by the trends from level density systematics at low energies, the latter is more appropriate and gives a reliable description of the magnitudes of level densities over a significant energy range. The theoretical description of level densities from [26] adequately described some but not all of the data. Additional studies in this mass region and extended to higher energies would be desirable.

ACKNOWLEDGMENTS

Discussions with P. Decowski are gratefully acknowledged. This work was funded in part by the United States National Science Foundation.

APPENDIX: ^{28}Si+^{165}Ho ER CROSS SECTIONS

Residue cross sections for ^{28}Si+^{165}Ho are presented in Fig. 7. Using the parameter descriptions extracted from the charged particle spectra, SM predictions are com-

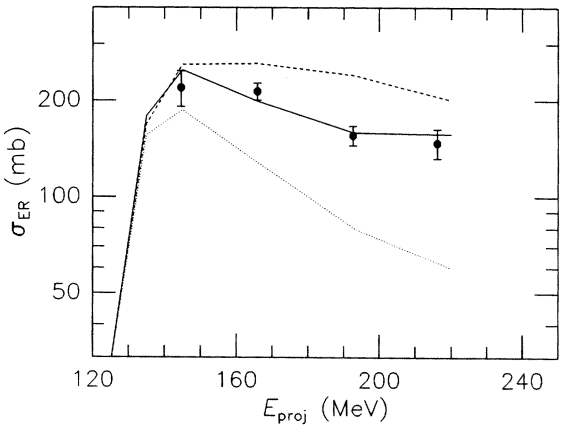

FIG. 7. ^{28}Si+^{165}Ho measured and calculated $\sigma_{\rm ER}$. SM calculations use $\tilde{a}_f/\tilde{a}_n = 1.02$, with 0.9×RFRM barriers and no presaddle delay (solid), 0.9×RFRM barriers and a 9×10^{-21} s presaddle delay (dashed), and temperature-dependent barriers and no presaddle delay (dotted). Calculations including delay with either temperature-dependent barriers and $\tilde{a}_f/\tilde{a}_n = 1.02$ or 0.9×RFRM barriers and $\tilde{a}_f/\tilde{a}_n$ increased to 1.04 give results similar to the solid curve.

pared with the data. The effects of modifying parameters which specifically affect the fission competition were explored.

Taking $\tilde{a}_f/\tilde{a}_n = 1.02$ and using RFRM fission barriers reduced by 10% results in a satisfactory description of the data. Imposing a 9×10^{-21} s presaddle fission delay as described in the recent work by Lestone *et al.* [32], the calculated excitation function is raised above the measured values as shown. Increasing $\tilde{a}_f/\tilde{a}_n$ slightly to 1.04 compensates and brings the prediction back in line with the data. This value is still well within conventional limits and it illustrates the well-known sensitivity to very small variation in $\tilde{a}_f/\tilde{a}_n$.

Alternatively, a reduction of fission barriers with temperature, as suggested by Newton *et al.* [63], can also have a dramatic influence on ER survival. By itself, this effect causes the predicted ER cross section to decrease too rapidly with energy. In combination with the fission delay, and keeping $\tilde{a}_f/\tilde{a}_n = 1.02$, the data can again be described well.

In summary, the ER cross section data by itself cannot be used to confirm (or to preclude) current ideas about dynamical delay times or temperature-dependent fission barriers within the present uncertainties of the SM.

[1] R. G. Stokstad, in *Treatise on Heavy-Ion Science*, edited by D. A. Bromley (Plenum, New York, 1985), Vol. 3, p. 83.

[2] N. G. Nicolis and D. G. Sarantites, Phys. Rev. C **40**, 2422 (1989).

[3] G. Viesti, B. Fornal, D. Fabris, K. Hagel, J. B. Natowitz, G. Nebbia, G. Prete, and F. Trotti, Phys. Rev. C **38**, 2640 (1988).

[4] W. E. Parker, M. Kaplan, D. J. Moses, G. La Rana, D. Logan, R. Lacey, J. M. Alexander, D. M. de Castro Rizzo, P. DeYoung, R. J. Welberry, and J. T. Boger, Phys. Rev. C **44**, 774 (1991).

[5] H. Ikezoe, N. Shikazono, Y. Nagame, Y. Sugiyama, Y. Tomita, K. Ideno, I. Nishinaka, B. J. Qi, H. J. Kim, and A. Iwamoto, Phys. Rev. C **46**, 1922 (1992).

[6] U. Gollerthan, T. Brohm, H.-G. Clerc, E. Hanelt, M. Horz, W. Morawek, W. Schwab, K.-H. Schmidt, F. P. Heßberger, G. Münzenberg, V. Ninov, R. S. Simon, J. P. Dufour, and M. Montoya, Z. Phys. A **338**, 51 (1991).

[7] J. M. Alexander, M. T. Magda, and S. Landowne, Phys. Rev. C **42**, 1092 (1990).

[8] N. G. Nicolis, D. G. Sarantites, L. G. Sobotka, and R. J. Charity, Phys. Rev. C **45**, 2393 (1992).

[9] J. R. Huizenga and L. G. Moretto, Ann. Rev. Nucl. Sci. **22**, 427 (1972).

[10] W. Reisdorf, Z. Phys. A **300**, 227 (1981); W. Reisdorf and J. Tõke, *ibid.* **302**, 183 (1981).

[11] J. Tõke and W. J. Swiatecki, Nucl. Phys. **A372**, 141 (1981).

[12] A. V. Ignatyuk, G. N. Smirenkin, and A. S. Tishin, Yad. Fiz. **21**, 485 (1975) [Sov. J. Nucl. Phys. **21**, 255 (1975)].

[13] S. K. Kataria, V. S. Ramamurthy, and S. S. Kapoor, Phys. Rev. C **18**, 549 (1978).

[14] K.-H. Schmidt, H. Delagrange, J. P. Dufour, N. Cârjan, and A. Fleury, Z. Phys. A **308**, 215 (1982).

[15] S. E. Woosley, in *Theory and Practice of Moment Methods in Many Fermion Systems*, edited by B. J. Dalton, S. M. Grimes, J. P. Vary, and S. A. Williams (Plenum, New York, 1980), p. 61.

[16] G. La Rana, R. Moro, A. Brondi, P. Cuzzocrea, A. D'Onofrio, E. Perillo, M. Romano, and F. Terrasi, Phys. Rev. C **40**, 2425 (1989).

[17] M. Kildir, G. La Rana, R. Moro, A. Brondi, A. D'Onofrio, E. Perillo, V. Roca, M. Romano, F. Terrasi, G. Nebbia, G. Viesti, and G. Prete, Phys. Rev. C **46**, 2264 (1992).

[18] A. Chbihi, L. G. Sobotka, N. G. Nicolis, D. G. Sarantites, D. W. Stracener, Z. Majka, D. C. Hensley, J. R. Beene, and M. L. Halbert, Phys. Rev. C **43**, 666 (1991).

[19] J. L. Wile, S. S. Datta, W. U. Schröder, J. Tõke, D. Pade, S. P. Baldwin, J. R. Huizenga, B. M. Quednau, R. T. deSouza, and B. M. Szabo, Phys. Rev. C **47**, 2135 (1993).

[20] H. Ikezoe, N. Shikazono, Y. Nagame, Y. Sugiyama, Y. Tomita, K. Ideno, A. Iwamoto, and T. Ohtsuki, Phys. Rev. C **42**, R1187 (1990).

[21] W. Kühn, P. Chowdhury, R. V. F. Janssens, T. L. Khoo, F. Haas, J. Kasagi, and R. M. Ronningen, Phys. Rev. Lett. **51**, 1858 (1983).

[22] S. Henss, A. Ruckelshausen, R. D. Fischer, W. Kühn, V. Metag, R. Novotny, R. V. F. Janssens, T. L. Khoo, D. Habs, D. Schwalm, D. Freeman, G. Duchène, B. Haas, F. Haas, S. Hlavac, and R. S. Simon, Phys. Rev. Lett. **51**, 11 (1988).

[23] J. Galin, B. Gatty, D. Guerreau, U. C. Schlotthauer-Voos, and X. Tarrago, Phys. Rev. C **10**, 638 (1974).

[24] B. Fornal, F. Gramegna, G. Prete, G. Nebbia, R. Smith, G. D'Erasmo, L. Fiore, A. Pantaleo, G. Viesti, P. Blasi, F. Lucarelli, I. Iori, and A. Moroni, Phys. Rev. C **41**, 127 (1990).

[25] S. Shlomo and J. B. Natowitz, Phys. Lett. B **252**, 187 (1990).

[26] S. Shlomo and J. B. Natowitz, Phys. Rev. C **44**, 2878 (1991).

[27] K. Hagel, D. Fabris, P. Gonthier, H. Ho, Y. Lou, Z. Majka, G. Mouchaty, M. N. Namboodiri, J. B. Natowitz, G. Nebbia, R. P. Schitt, G. Viesti, R. Wada, and B. Wilkins, Nucl. Phys. **A486**, 429 (1988).

[28] M. Gonin, L. Cooke, K. Hagel, Y. Lou, J. B. Natowitz, R. P. Schmitt, B. Srivastava, W. Turmel, H. Utsonomiya, R. Wada, B. Fornal, G. Nardelli, G. Nebbia, G. Viesti, R. Zanon, G. Prete, P. Gonthier, and B. Wilwins, Phys. Lett. B **217**, 406 (1989).

[29] D. J. Hinde, D. Hilscher, and H. Rossner, Nucl. Phys. **A502**, 497c (1989).

[30] J. P. Lestone, J. R. Leigh, J. O. Newton, J. X. Wei, J. X. Chen, S. Elfström, and M. Zielinska-Pfabé, Nucl. Phys. **A559**, 277 (1993).

[31] D. J. Hinde, D. Hilscher, H. Rossner, B. Gebauer, M. Lehmann, and M. Wilpert, Phys. Rev. C **45**, 1229 (1992).

[32] J. P. Lestone, Phys. Rev. Lett. **70**, 2245 (1993).

[33] K.-T. Brinkmann, A. L. Caraley, B. J. Fineman, N. Gan, J. Velkovska, and R. L. McGrath, Phys. Rev. C **50**, 309 (1994).

[34] P. A. DeYoung, R. L. McGrath, and W. F. Piel, Jr., Nucl. Instrum. Methods **226**, 555 (1984).
[35] B. J. Fineman, K.-T. Brinkmann, A. L. Caraley, N. Gan, W. J. Kernan, and R. L. McGrath, The Nuclear Structure Laboratory Progress Report 1990-1992, Stony Brook, 1992, p. 96ff (unpublished).
[36] J. Wilczynski, K. Siwek-Wilczynska, J. van Driel, S. Gonggrijp, D. C. J. M. Hageman, R. V. F. Janssens, J. Lukasiak, and R. H. Siemssen, Phys. Rev. Lett. **45**, 606 (1980).
[37] T. C. Awes, S. Saini, G. Poggi, C. K. Gelbke, and D. Cha, Phys. Rev. C **25**, 2361 (1982).
[38] F. Pühlhofer, Nucl. Phys. **A280**, 267 (1977).
[39] M. Herman, U. of Rochester Nuclear Structure Laboratory Report No. UR-NSRL-318, 1987 (unpublished).
[40] T. Sikkeland, Phys. Rev. **135**, B669 (1964).
[41] B. B. Back, R. R. Betts, J. E. Gindler, B. D. Wilkins, S. Saini, M. B. Tsang, C. K. Gelbke, W. G. Lynch, M. A. McMahan, and P. A. Baisden, Phys. Rev. C **32**, 195 (1985).
[42] D. J. Hinde, J. O. Newton, J. R. Leigh, and R. J. Charity, Nucl. Phys. **A398**, 308 (1983).
[43] D. Wilmore and P. E. Hodgson, Nucl. Phys. **55**, 673 (1964).
[44] F. G. Perey, Phys. Rev. **131**, 745 (1963).
[45] L. McFadden and G. R. Satchler, Nucl. Phys. **84**, 177 (1966).
[46] J. R. Huizenga, A. N. Behkami, I. M. Govil, W. U. Schröder, and J. Tõke, Phys. Rev. C **40**, 668 (1989).
[47] D. W. Lang, Nucl. Phys. **77**, 353 (1963), J. D. W. Lang, Proc. Phys. Soc. London A **67**, 585 (1954).
[48] M. Kicińska-Habior, K. A. Snover, J. A. Behr, G. Feldman, C. A. Gosset, and J. H. Gundlach, Phys. Rev. C **41**, 2075 (1990).
[49] S. Cohen, F. Plasil, and W. J. Swiatecki, Ann. Phys. (N.Y.) **82**, 557 (1974).
[50] A. J. Sierk, Phys. Rev. C **33**, 2039 (1986).
[51] E. M. Rastopchin, Yu. B. Ostapenko, M. I. Svirin, and G. N. Smirenkin, Yad. Fiz. **49**, 24 (1989) [Sov. J. Nucl. Phys. **49**, 15 (1989)].
[52] A. V. Ignatyuk, M. G. Itkis, V. N. Okolovich, G. N. Smirenkin, and A. S. Tishin, Yad. Fiz. **21**, 1185 (1975) [Sov. J. Nucl. Phys. **21**, 612 (1975)].
[53] D. J. Hinde, J. R. Leigh, J. O. Newton, W. Galster, and S. Sie, Nucl. Phys. **A385**, 550 (1982).
[54] N. G. Nicolis, D. G. Sarantites, C. Baktash, V. Abenante, L. A. Adler, J. R. Beene, F. A. Dilmanian, G. Garcia-Bermudez, H. C. Griffin, M. L. Halbert, D. C. Hensley, N. R. Johnson, I. Y. Lee, Z. Majka, F. K. McGowan, M. A. Riley, T. M. Semkow, D. W. Stracener, and A. Virtanen, Nucl. Phys. **A520**, 153c (1990).
[55] W. Morawek, D. Ackermann, T. Brohm, H.-G. Clerk, U. Gollerthan, E. Hanelt, M. Horz, W. Schwab, B. Voss, K.-H. Schmitt, and F. P. Heßberger, Z. Phys. A **341**, 75 (1991).
[56] F. P. Heßberger, V. Ninov, and D. Ackermann, Z. Phys. A **343**, 301 (1992).
[57] H. Feldmeier, Dynamics of Dissipative Heavy-Ion Reactions, in *Nuclear Structure and Heavy Ion Dynamics*, edited by L. Moretto and R. A. Ricci (North-Holland, Amsterdam, 1984), p. 274.
[58] H. Feldmeier, Rep. Prog. Phys. **50**, 915 (1987).
[59] J. J. Gaardhøje, Annu. Rev. Nucl. Part. Sci. **42**, 483 (1992).
[60] P. A. DeYoung, C. J. Gelderloos, D. Kortering, J. Sarafa, K. Zienert, M. S. Gordon, B. J. Fineman, G. P. Gilfoyle, X. Lu, R. L. McGrath, D. M. de Castro Rizzo, J. M. Alexander, G. Auger, S. Kox, L. C. Vaz, C. Beck, D. J. Henderson, D. G. Kovar, and M. F. Vineyard, Phys. Rev. C **41**, R1885 (1990).
[61] P. Fröbrich and I. I. Gontschar, Nucl. Phys. **A563**, 326 (1993).
[62] T. Wada, Y. Abe, and N. Carjan, Phys. Rev. Lett. **70**, 3538 (1993).
[63] J. O. Newton, D. G. Popescu, and J. R. Leigh, Phys. Rev. C **42**, 1772 (1990).